Article type: Original Paper

Generation of multi-gigahertz trains of phase-coherent femtosecond laser pulses in Ti:sapphire waveguides

Christos Grivas[1,2], Rand Ismaeel[3], Costantino Corbari[3], Chung-Che Huang[3], Dan W. Hewak[3], Pavlos Lagoudakis[2,4], Gilberto Brambilla[3]*

*Corresponding Author: E-mails: chr.grivas@gmail.com & grivas@kth.se

[1] KTH – Royal Institute of Technology, School of Engineering Sciences, Department of Applied Physics, Stockholm SE-10691, Sweden
[2] Department of Physics and Astronomy, University of Southampton, Southampton SO17 1BJ, UK
[3]Optoelectronics Research Centre, University of Southampton, Southampton SO17 1BJ, UK
[4] Skolkovo Institute of Science and Technology, Novaya St., 100, Skolkovo 143025 Russian Federation

Miniature lasers producing ultrashort phase-coherent pulses at high repetition rates by stable mode-locking in ambient conditions can offer unique capabilities in various applications, spanning from microwave photonics to telecom and biological imaging techniques. Here, the operation of graphene mode-locked lasers based on channel waveguides written by femtosecond and picosecond laser pulses in Ti:sapphire crystals is demonstrated. Trains of pulses of 41.4-fs duration at a 21.25-GHz repetition rate were generated by capitalizing on the formation of solitons in their monolithic resonators through Gires–Tournois interferometers. The latter, allow for effective pulse shaping via tuning of the intracavity group delay dispersion while simultaneously enabling ultralow laser operating thresholds. A number of features of these sources, including their high-brightness and broad bandwidth, are essential ingredients for achieving high longitudinal resolution and sensitivity, which are the primary performance metrics of the Fourier domain/spectral domain variant of optical coherence tomography systems. A further doubling of the laser repetition rate to 42.5 GHz was achieved by coherent pulse interleaving in optical fiber technology, thereby underlining the potential of the Ti:sapphire waveguide lasers to produce highly stable, wide-spaced combs of phase-coherent optical frequency lines.

1. Introduction

Ti:sapphire crystals with their broad gain bandwidths[1] have enabled the advancement of the frontiers in the technologies of ultrashort-pulse and broadly wavelength tunable lasers,[2] enabling generation of pulses with durations as short as 5 fs.[3–5] The possibility of alleviating the effect of short fluorescence lifetimes and low emission cross sections of the Ti^{3+} ions in these crystals and, in turn, of reducing the inherently high thresholds of Ti:sapphire bulk lasers has motivated strong interest in exploiting the confinement of the laser and pump modes in optical waveguides. In this respect, the adoption of planar slab[6] and channel[7–11] as well as fiber[12,13] waveguide geometries led to the development of Ti:sapphire continuous wave (c.w.) lasers[6,8–10,13] and broadband and high-brightness light sources.[7,11,12]

Although, from an application viewpoint, high-repetition-rate, femtosecond Ti:sapphire waveguide lasers are appealing in various areas, including photobiology and photo-medicine there has been no report, to date, on their mode-locking. To this end, passive mode-locking, represents an attractive technology for the generation of low jitter, ultra-short pulses at multi-GHz repetition rates as its realization relies on short, mechanically stable monolithic waveguide cavities.[14] In diagnostic imaging modalities such as Fourier-domain optical coherence tomography (FDOCT), particularly its spectral-domain (SDOCT) variant, which dominates in the wavelength range 780-850 nm, the short coherence lengths of these ultra-high bandwidths sources would enable sub-cellular scale axial resolutions and in turn enhanced imaging quality of internal tissue microstructures. Another approach that has evolved in parallel to SDOCT is the swept-source OCT (SSOCT), which prevails in the spectral ranges around 1050 nm and 1300 nm and relies on the use of rapidly tuned, narrow linewidth lasers, thereby allowing high imaging speeds.[15–17] To date, bulk femtosecond Ti:sapphire lasers are considered to be archetypical sources for OCT having enabled ultrahigh resolution imaging of live cells/tissues.[18] With a view to developing miniaturized diagnostic instruments, all

aforementioned applications could also greatly benefit from the availability of compact light sources that offer promise for on-chip or on-board integration with detection units.

A scope for reduction of the pulsewidths and generation of high-intensities in passively mode-locked lasers is offered by soliton mode-locking, in which the time-dependent nonlinear pulse phase shift induced by the self-phase modulation (SPM) is compensated by balancing the dispersive and nonlinear lengths in the cavity. A favorable feature of such implementations is that the critical pulse energy required for the onset of mode-locking is significantly lower than in the non-soliton regime, thereby reducing the tendency of these lasers to exhibit Q-switching instabilities.[19] It is noted that in this mode-locking approach, the saturable absorber serves simply as a means of triggering and stabilizing the pulsation rather than of pulse shaping.

In this article, we report on the soliton mode-locked laser operation of femtosecond (fs) - and picosecond (ps)-laser-written Ti:sapphire channel waveguides at the fundamental frequency of 21.25 GHz, using a graphene layer as a saturable absorber. Researchers in recent years have increasingly capitalized on the use of ultra-short laser pulses, typically of a few tens of femtosecond duration, as a fabrication tool for the development of waveguide-based, integrated photonic devices,[20–22] which in the case of Ti:sapphire crystals include waveguide lasers,[10] broadband fluorescence sources,[11] and beam splitters.[23] Here, we extended the range of pulsewidths by an order of magnitude to include also pulses with ps duration. Aside from its large nonlinear absorption as well as low cost and facile fabrication, the main advantage of graphene with respect to other types of saturable absorbers is arguably that it can be used over an ultrabroad wavelength range, despite its wavelength dependent performance[24]. The suitability of graphene saturable absorbers (GSAs) for the mode-locking of Ti:sapphire lasers, has been demonstrated in extended cavity formats leading to the generation of 63-fs pulses at a repetition rate of 99.4 MHz[25]. In the mode-locking scheme applied here, soliton pulses of duration as short as 41.4 fs could be generated by tuning the intracavity group delay dispersion

(GDD) with an equivalent to a Gires-Tournois interferometer (GTI) formed between the saturable absorber and one of the waveguide endfaces.[26–28] Furthermore, we demonstrate rate multiplication by a factor of two, to 42.5 GHz, the highest reported for a waveguide laser to date, by coherent pulse interleaving in optical fiber technology using an asymmetric Mach-Zehnder interferometer (MZI) with a suitably tailored delay line in one of its arms. This route for repetition rate scaling is associated with a filtering effect in the frequency domain and represents an alternative to the one involving Fabry-Perot cavities.[29]

2. Materials and experimental methods

2.1. Development of Ti:sapphire channel waveguides

For the inscription of channel waveguides in the fs- and ps-regime, the outputs from a mode-locked regenerative amplified KGW:Yb^{3+} laser (1030 nm, 180 fs, 1 KHz, 1.5 μJ) and a YVO_4:Nd^{3+} laser (1064 nm, 8 ps, 200 kHz) were used, respectively.[10] The channels were defined in the bulk of a 0.12 wt% Ti:sapphire crystal by pairs of parallel lines, which acted as optical barriers and were separated by a distance of 24 μm, which is the optimum value to ensure near-diffraction-limited emission. The lines were formed ~150 μm below the crystal surface by focusing the writing laser pulses through a microscope objective lens with a numerical aperture of 0.65. Cross-sectional images of two waveguides written with fs- and ps-laser pulses are displayed in **Figures 1a** and **1b** respectively, indicating that the corresponding depths of the defining lines were 15.7 μm and 9.7 μm. The stress that developed the area in-between and along the lengths of each pair of lines resulted in an increase in the refractive index with respect to that of the host crystal, and in turn in mode confinement and light guidance. During the writing process, the crystal, which had its plane perpendicular to its crystallographic c-axis, was scanned transversally to the incident laser pulses such that the light polarization was parallel to the writing direction. The combination of the polarization of the writing beam and

the orientation of the crystallographic axis of the host crystal was chosen such that a potential formation of nanogratings in the guiding area would not compromise the laser performance. Formation of such nanostructures has been observed in glasses[30,31] and more recently in Ti:sapphire[32] and undoped sapphire crystals,[33] leading to scattering of the launched beam if its polarization is parallel to that of the writing beam. The writing direction was the same for the two lines of each pair to prevent a potential differentiation in the modification of the material as a result of the opposite writing directions within the bulk of the non-centrosymmetric crystal.[34] The scanning speeds, v_{SC}, used in the fs and ps laser writing regime were 15 μm·s^{-1} and 0.5 mm·s^{-1}, respectively, while the corresponding pulse energies, E_p, 1.5 μJ and 0.3 μJ. After the completion of the laser writing process, the waveguide endfaces were polished to an optical finish and a length of 4 mm.

2.2. Experimental setup for soliton mode-locking experiments

A schematic of the experimental setup for the demonstration of mode-locked operation is shown in **Figure 1c**. The channel waveguides were optically pumped at 532 nm by a diode-pumped solid-state laser (DPSS). The electric field of the π-polarized pump beam was parallel to the crystallographic c-axis and coupled to the channels with a 16x microscope objective. To estimate an upper limit for their propagation loss, lasing in the waveguides was first obtained in c.w. mode by using the arrangement shown in Figure 1c and forming their resonators with two highly reflective (HR) mirrors (R = 99.5%) attached to their end-faces. From the experimentally derived slope efficiencies propagation losses of 0.65 dB·cm^{-1} and 1.8 dB·cm^{-1} were calculated in waveguides inscribed by fs and ps laser pulses, respectively, at the signal wavelength of 798.5 nm (for details see Supporting information). The higher loss in the ps-laser-writing regime is due to the stronger interaction of the modal field with the defining lines of the guides. This, in turn, results from the rougher type of material modification and the larger magnitude of the entailed negative index change, of the order of 2.7×10^{-3} as compared to 1 ×

10^{-3} in the fs-laser-writing regime.[10] The laser cavities used for mode-locking was formed by attaching at the front-endface of the waveguides a thin mirror with a reflectivity of R_{OC}=96.5% at the signal wavelength, which served both as an incoupling and outcoupling mirror. A second, highly reflective (HR, R_B=99.5%) mirror coated by a graphene layer (for fabrication details see Supporting Information) that acted as a saturable absorber was mounted on a piezoelectric stage and brought in close proximity to the waveguide back-endface. To achieve soliton mode-locking, the cavity dispersion was modulated by varying the gap between the waveguide back endface and the GSA/mirror complex, which formed a GTI. The laser output was separated from the pump radiation by a dichroic beam splitter.

**********FIGURE 1**********

3. Results

3.1. Graphene-mode locked Ti:sapphire waveguide lasers.

To determine the parameters of the GSA that are critical for the mode-locked operation the impact of the incident pulse energy fluence on its transmission was studied using an optical oscillator (Coherent-Chameleon), yielding ~200 fs pulses at λ_L = 798.5 nm and a repetition rate of 80 MHz. As shown on a logarithmic scale in **Figure 2**, at the wavelength of 798.5 nm the GSA transmission increases from the level of its linear transmission, T_{lin} = 96.1% (see Supporting Information) at low fluence settings, to the saturation level, T_{sat} = 98.2% for infinitely high fluences. From a fitting to the data obtained, both the modulation depth, $\Delta q = T_{sat} - T_{lin}$, and the saturation fluence, $F_{sat,A}$, defined as the pulse energy fluence required for the transmission of infinitely thin absorbers to increase by 37% with respect to T_{lin}, were determined to be 67 $\mu J \cdot cm^{-2}$ and 2.1%, respectively. From Figure 2, the value derived for the nonsaturable loss α_{GSA}, that is, the difference between full transmission (T = 1) and the transmission that corresponds to the saturation level, T_{sat}, is 1.8%.

**********FIGURE 2**********

To study the mode-locked operation of the Ti:sapphire waveguide lasers, the RF spectra of their output were recorded using an ultrafast InGaAs photodiode with a 45-GHz bandwidth connected to an RF spectrum analyzer. **Figure 3a** shows a narrow frequency span (100 MHz) RF spectrum of the fundamental repetition frequency of $f_R \sim 21.25$ GHz. Considering that the latter is inversely proportional to the cavity length and described by

$$f_R = \frac{c}{2 \cdot n \cdot L_{cav}} \quad (1)$$

we derive from **Equation 1** for the monolithic Ti:sapphire waveguide cavity with a length of $L_{cav} = 4$ mm, which is equal to the length of the waveguide, and a refractive index of $n = 1.765$, an operating frequency f_R equal to the experimentally obtained one. The peak exhibits a signal-to-noise ratio of 60 dB, indicating stable c.w. mode-locked operation without any evidence of Q-switching instabilities. Similar results that point to stable mode-locking were also obtained from sources developed with ps-laser-irradiation, as they exhibit signal-to-noise ratios in excess of 56 dB. The repetition rate of the fundamentally mode-locked waveguide lasers was also determined by recording the autocorrelation and the first cross-correlations with adjacent pulses, shown in **Figure 3b**, and measuring the peak-to-peak spacing. The latter is 47.06 ps, thereby confirming that the repetition rate is indeed 21.25-GHz. The slightly lower intensities of the cross-correlations are attributed to the higher loss of the autocorrelator for large delays.

**********FIGURE 3**********

Further characterization of the mode-locked pulse trains involved measurement of their auto-correlation and the optical spectra. Figures 3c and 3d show intensity autocorrelation traces with full-width at half-maximum (FWHM) values of $\tau_{FWHM}^{(fs)} = 63.7$ fs and $\tau_{FWHM}^{(ps)} = 87.1$ fs, obtained from the Ti:sapphire waveguide lasers inscribed by pulses with fs- and ps-duration, respectively, at their maximum output powers of 108.4 mW and 53.5 mW yielded by. Assuming hyperbolic secant ($sech^2$) pulse shapes, the respective pulsewidths derived are $\Delta\tau_{(fs)} = 41.4$ fs

and $\Delta\tau_{(ps)}$ = 56.6 fs. Figures 3c and 3d also include the optical spectra of the corresponding pulse trains, indicating spectral FWHM bandwidths of $\Delta\lambda_{(fs)}$ = 18.4 fs and $\Delta\lambda_{(ps)}$ = 14.45 nm, at 798.5 nm. The time-bandwidth product (TBP) values of $\Delta\tau_{(fs)}\cdot\Delta\nu_{(fs)}$ = 0.358 and $\Delta\tau_{(ps)}\cdot\Delta\nu_{(ps)}$ = 0.384 derived, suggest generation of pulses close to transform limit.

Figure 4 shows the input-output characteristics of channel waveguide lasers developed with the use of femtosecond (picosecond) laser pulses, indicating a threshold of 72 mW (128.8 mW) with respect to the absorbed pump power for the c.w. laser oscillation. Higher absorbed pump powers, exceeding 550 mW (1040 mW), triggered Q-switched mode-locked operation, whilst stable soliton mode-locking was achieved above the threshold value of 1160.1 mW (1465.6 mW), allowing for the generation of an average output power of 87.48 mW (51.25 mW). As aforementioned, a maximum average output power of 108.4 mW (53.5 mW) was obtained for an absorbed pump power of 1446 mW (1500.45 mW). We note that the fs-laser-inscribed waveguide shows superior laser performance compared to its ps-laser-written counterpart due to its lower propagation loss.

**********FIGURE 4**********

The intracavity GDD and in turn the mode-locking stability is critically dependent on the size of the GTI air-filled gap[35] (see Supporting Information). The selection of the gap size calls for simultaneously addressing the needs on one hand for fully balancing of the second order dispersion and the SPM to avoid the formation of chirped pulses, and on the other hand for preventing excessive loss due to diffraction in free space. Next, the intracavity GDD values per roundtrip required for the generation of pulses with FWHM duration of $\tau_{\mathrm{FWHM}}^{(fs)}$ = 63.7 fs and $\tau_{\mathrm{FWHM}}^{(ps)}$ = 87.1 fs in the fs-laser- and ps-laser-written channel waveguides, respectively, are derived from the soliton theorem equation

$$\tau_{\mathrm{FWHM}} = \left(\frac{2 \cdot 1.76 \cdot |\mathrm{GDD}|}{\gamma_{\mathrm{SPM}} \cdot \mathrm{E}_{\mathrm{CAV}}}\right) \qquad (2)$$

Here, GDD includes contributions from the material dispersion in the Ti:sapphire crystal and the air gap in the GTI structures, whereas the terms E_{CAV} and γ_{SPM} stand for the intracavity pulse energy and the SPM coefficient per round trip, respectively, and are given by the following expressions

$$E_{CAV} = \frac{P_{CAV}}{f_R} = \frac{P_{OUT}}{(1 - R_{OC}) \cdot f_R} \quad (3)$$

$$\gamma_{SPM} = \left(\frac{4 \cdot n_2 \cdot \pi \cdot L_{rt}}{A_{eff,L} \cdot \lambda_L} \right) \quad (4)$$

In **Equations 3** and **4**, R_{OC} = 4.5% is the reflectivity of the outcoupling cavity mirror, P_{OUT} the average output power of the waveguide lasers, and $A_{eff,L}$ the effective beam size in the gain medium. As for the terms $n_2 = 3.3 \times 10^{-20}$ and L_{rt} = 8 mm, they represent the nonlinear refractive index and the round-trip propagation length in the gain medium, respectively. From Equation 3, it can be then calculated that for the fs- and ps-laser-written waveguides lasers at their respective maximum output powers, P_{OUT}, of 108.4 mW and 53.5 mW the corresponding E_{CAV} values are 113.4 pJ and 56.6 pJ. Finally, by introducing in Equation 4 the mode sizes $A_{eff,L}$ of each of the two lasers, namely 39.58 μm^2 (3.5 μm x 3.6 μm) and 37.38 μm^2 (3.4 μm x 3.5 μm), we obtain for the SPM coefficients the values $\gamma_{SPM(fs)} = 105\ \mu rad \cdot W^{-1}$ and $\gamma_{SPM(ps)} = 111\ \mu rad \cdot W^{-1}$, respectively. Considering that the material dispersion per roundtrip in the Ti:sapphire crystal is 530 fs^2, it can be derived from **Equation 2** that the contributions from the GTI effect in the two cavities are $GDD_{(fs)} = -600\ fs^2$ and $GDD_{(ps)} = -580\ fs^2$, respectively.

3.2. Soliton mode-locked laser thresholds

We next calculate the minimum E_{CAV} required for stable soliton c.w. mode-locking from **Equation 5** that describes the general condition for preventing Q-switching instabilities in ion-doped, soliton mode-locked lasers, and reads[19]

$$\left(F_{sat,L} \cdot A_{eff,L} \cdot g \cdot K^2 \cdot E_{CAV}^3 + E_{CAV}^2 \right)^{1/2} \geq E_{(cr)} \quad (5)$$

where $E_{(cr)}$ is the critical pulse energy representing the minimum intracavity pulse energy required to obtain stable c.w. mode-locking in the non-soliton regime[19]

$$E_{(cr)} = \left(F_{sat,L} \cdot A_{eff,L} \cdot F_{sat,A} \cdot A_{eff,A} \cdot \Delta q \right)^{1/2} \quad (6)$$

where F_{sat} and A_{eff} are the saturation fluences and the effective laser mode areas in the gain medium (L) and the saturable absorber (A), respectively. In **Equation 6**, the term $A_{eff,A}$ can be approximated as being equal to $A_{eff,L}$, which, as aforementioned, was measured to be 39.58 μm^2 and 37.38 μm^2 in fs- and ps-laser written channels, respectively. Finally, in the same equation, $F_{sat,A}$ = 67 $\mu J \cdot cm^{-2}$ and $F_{sat,L}$ = 2.648 x 10^3 $J \cdot m^{-2}$ as derived from the expression:

$$F_{sat,L} = \frac{h \cdot v}{m \cdot \left(\sigma_{em} + \sigma_{abs}^{L} \right)} \quad (7)$$

where, $h \cdot v$ is the photon energy, m = 2 represents the number of passes through the gain medium within one round trip, while σ_{em} = 41 x 10^{-24} m^{-2} and σ_{abs}^{L} = 6 x 10^{-24} m^{-2} are the emission and absorption cross sections of the Ti:sapphire crystal at the laser wavelength, respectively. By introducing the above values in Equation 6, we calculated that a minimum intracavity energy of $E_{(cr)}$ = 242 pJ (228 pJ) is required for mode-locking in the non-soliton regime the waveguide laser fabricated by fs- (ps-) laser writing.

Returning to Equation 5, the term K represents the variation of the ratio of the pulse bandwidth, $\Delta\nu$, to the gain bandwidth, $\Delta\nu_g$, with the E_{CAV}, and is given by

$$K = \frac{\Delta\nu}{\Delta\nu_g} = \left(\frac{2 \cdot \pi \cdot n_2 \cdot L_{CAV}}{A_{eff,L} \cdot \lambda_L \cdot |GDD| \cdot \Delta\nu_g} \right) \cdot \left(\frac{TBP}{1.76} \right) = \left(\frac{\gamma_{SPM}}{|GDD| \cdot \Delta\nu_g} \right) \cdot \left(\frac{TBP}{1.76} \right) \quad (8)$$

where TBP stands for the experimentally obtained time-bandwidth-products of the fs- and ps-laser-written waveguide lasers, being, as aforementioned, 0.358 and 0.384, respectively. With regard to the gain bandwidth $\Delta\nu_g$ in **Equation 8**, for both types of waveguides, a value of 75 THz was estimated from the FWHM values of Gaussian fittings to the central parts the

corresponding fluorescence spectra. Finally, the term g in Equation 5 is the time-dependent round-trip power gain when the pulse maximum is reached. In this case, g equals the linear losses that is, the round-trip cavity loss obtained from the expression

$$g = ln\left(\frac{1}{R_{OC} \cdot R_1 \cdot (1-\alpha_{WG}) \cdot (1-\alpha_{GSA})^2}\right) \quad (9)$$

where α_{WG} is the round-trip propagation loss in the Ti:sapphire waveguides, being 11.3% and 28.2% for channels written in the fs- and ps-regime, respectively (See Supporting Information). The term $(1-\alpha_{GSA})^2$, represents the loss arising from the double-pass through the GSA due to its non-saturable loss α_{GSA}= 1.8%, as derived from Figure 2. From **Equation 9** it can be estimated that the g values for waveguides fabricated by fs- and ps-laser pulses are 0.207 and 0.419, respectively.

By introducing into the Equation 5 the values derived for all its parameters, the minimum intracavity pulse energies required to overcome Q-switching instabilities in waveguides fabricated in the fs- (ps-) laser writing regime were calculated to be E_{CAV} = 83.1 pJ (48.6 pJ). Notably, these value are less than half (one fourth) of the corresponding energies derived from Equation 6 for the non-soliton mode-locking regime, being as aforementioned, $E_{(cr)}$ = 242 pJ (228 pJ). Furthermore they are consistent with the experimental values of 91.5 pJ (53.6 pJ) for stable soliton mode-locking, which can be obtained by introducing in Equation 3, the respective output powers measured at the threshold for stable cw mode-locking of 87.48 mW (51.25 mW).

3.3. Coherent pulse interleaving for rate multiplication.

Although waveguide lasers with their small cavity footprints open up the possibility of operation at high fundamental repetition frequencies, further scaling to higher values is limited by the absorption length of the gain medium, which is effectively the minimum length that the cavity can acquire without compromising the maximum achievable optical gain. One real

option for repetition frequency scaling beyond the limits set by the monolithic cavity length is the implementation of optical interleaving technologies. Here, we realized coherent pulse interleaving for rate multiplication by a factor of 2 to 42.5 GHz, which corresponds to a free spectral range (FSR) in terms of wavelength separation, of 109.4 pm. To this end, we used an optical interleaver filter based on two directional microcouplers with 50:50 power splitting ratio[36], formed using a single mode (780 - 970 nm) silica fiber asymmetric MZI (for fabrication details see Supporting Information), schematically shown in **Figure 5a**. The laser pulse train from a mode-locked laser developed by fs-laser writing was coupled into the interleaver, where it was divided into two parts by a 50:50 splitter. Taking into account that the effective index of the silica glass fiber at the lasing wavelength is n_{eff} = 1.457, a delay line with a length of $\Delta z \sim$ 4.846 mm, which is given by

$$\Delta z = \frac{c \cdot \Delta\tau}{n_{eff}} \tag{10}$$

was introduced into one of the 70-mm-long arms of the MZI in order to ensure that the propagating pulses experience a time delay $\Delta\tau \sim$ 23.53 ps that is equal to half the repetition period of the input pulse train

$$\Delta\tau = \frac{1}{2 \cdot f_R} \tag{11}$$

The two MZI arms were re-combined, resulting in the doubling of the input repetition rate.

**********FIGURE 5**********

Optical characterization of the interleaver in terms of transmission, linear losses, and suppression levels was performed with a tunable, narrow-linewidth (< 75 kHz) Ti:sapphire probe laser (MRB-110, Coherent). To compensate fabrication tolerances and potential deviations from the 50:50 splitting ratio and the optimal delay line length, which can lead to a mismatch of the repetition rate f_R and the filter spacing and in turn to phase-incoherent output pulses, the coupler and the delay line were thermally tuned, as indicated in Figure 5a. The

optical transmission spectrum of the interleaver shown in **Figure 5b**, exhibits a maximum side-mode suppression of 22.1 dB and was recorded by modulating the wavelength of the narrow-linewidth probe laser over the range from 798.45 nm to 799.75 nm with a step of 1 pm, whilst the interleaver filter was thermally tuned. However, it is noted that the suppression measured does not represent the actual depth of the interleaver notches, which correspond to the minima in the transmission spectrum and remained most likely undetected due to the relatively large wavelength-tuning step. As the length of the longest arm of the directional coupler is 74.846 mm, we conclude that the propagation loss in the fiber, which is of the order of 3.65 $dB \cdot km^{-1}$ has a negligible contribution to the transmission loss. The latter originates primarily from the coupling losses of the waveguide laser output into the interleaver amounting to 1.55 dB, as indicated in Figure 5b. The overall transmission losses through the fiber interleaver are 1.9 dB, corresponding to an output power of 70 mW obtained for 108.4 mW of input power.

To evaluate the performance of the interleaved mode-locked waveguide laser the RF spectrum of the output pulse train was measured using a 45-GHz photodetector. During the measurement, the interleaver filter was thermally tuned to mitigate the adverse effects of any delay line offsets on the sidemode suppression. The spectrum obtained is shown in **Figure 5c**, revealing a suppression ratio of 44.2 dB, for the 42.5-GHz interleaved pulses. To confirm the repetition rate of the interleaved waveguide laser, we recorded its intensity autocorrelation trace over a large time window and measured the separations between the autocorrelation and the first correlations peaks, which, as indicated in **Figure 5d**, are 23.53 fs, corresponding indeed to a repetition rate of 42.5 GHz. **Figure 5e** shows the autocorrelation trace of a single interleaved pulse, indicating an FWHM value of $\tau_{\mathrm{FWHM}}^{(\mathrm{inter-exp})}$ = 150 fs, which by assuming a hyperbolic secant ($sech^2$) pulse shape, yields a pulsewidth of $\Delta\tau_{(\mathrm{inter})}$ = 97.5 fs. This longer FWHM duration with respect to that of the input pulses ($\tau_{\mathrm{FWHM}}^{(\mathrm{fs})}$= 63.7 fs) obtained directly from the waveguide laser is attributed to the GDD accumulated in the fiber MZI. To investigate the consistency of

the temporal pulse broadening measured, we next calculate the FWHM-duration of the interleaved pulses, $\tau_{(\mathrm{FWHM})}^{(\mathrm{inter-calc})}$. For this purpose, we use as an approximation the equation that provides the FWHM-duration of Gaussian pulses

$$\tau_{(\mathrm{FWHM})}^{(\mathrm{inter-calc})} = (\tau_{\mathrm{FWHM}}^{(\mathrm{fs})})^2 \cdot \left[1 + \left(2 \cdot \ln 2 \cdot \mathrm{GDD} \cdot \lambda^2 \Big/ \pi \cdot c \cdot (\tau_{\mathrm{FWHM}}^{(\mathrm{fs})})^2\right)^2\right]^{1/2} \qquad (12)$$

Considering that the group velocity dispersion (GVD) in the fiber used to fabricate the interleaver is 40 fs^2/mm, it follows that the GDD in the ~75-mm-long MZI arm that incorporates the delay line amounts to 3000 fs^2. According to **Equation 12**, this level of GDD would result in a temporal broadening of the input pulses from $\tau_{\mathrm{FWHM}}^{(\mathrm{fs})}$ = 63.7 fs to $\tau_{(\mathrm{FWHM})}^{(\mathrm{inter-calc})}$ = 145 fs, which is in good agreement with the experimentally obtained pulsewidth of $\tau_{\mathrm{FWHM}}^{(\mathrm{inter-exp})}$ = 150 fs.

The repetition rate drifts observed over a time span of 30 minutes were indiscernible thanks to the stability of the monolithic waveguide laser source and the low propagation loss in the interleaver filter. It is expected, therefore, that fluctuations in the carrier-envelope offset (CEO) frequency resulting from the difference between phase and group velocity in dispersive intracavity media are equally small.

4. Discussion and conclusions

We have demonstrated the generation of pulsed output with a duration as short as 41.4 fs in channel waveguides inscribed in the bulk of a Ti:sapphire crystal by direct laser writing with femtosecond and picosecond pulses via soliton mode-locking using graphene as a saturable absorber. Tailoring the GDD by means of a GTI in the waveguide cavity, as implemented here, offers the advantage of flexibility in terms of establishing any desired GDD level compared to integrated configurations. In the latter, dispersion compensation is achieved by interfacing the

waveguide gain medium with of a passive waveguide segment that provides the desirable GDD level[37,38]. The small footprint of the sources enabled operation at the fundamental frequency of 21.25 GHz, which is a record high value for waveguide lasers, with a maximum average output power in excess of 108 mW. Furthermore, we have highlighted the suitability of optical fiber interleaver filters based on Mach–Zehnder interferometers for scaling the repetition rate of the fundamentally mode-locked waveguide lasers by a factor of two, to the level of 42.5 GHz. There is scope for enhancement of laser performance in terms of both the pulse duration and output powers generated. Obtaining pulses with sub-20 fs duration is at present subject to limitations imposed by the third order dispersion in the Gires-Tournois structure. A possible way to circumvent this problem in the current monolithic resonator format is by using highly dispersive mirrors to form the waveguide cavity. Such mirrors can be designed to ensure broadband and, in effect high-order-dispersion-free GDD at the desired level.[39,40] Reducing the propagation loss in the waveguides will offer a route to achieving lower lasing thresholds and the higher output powers with the levels of absorbed pump powers reported in our work. Furthermore, the adoption of thermal management schemes will enable further output power scaling through the use of higher pump powers. Although in graphene mode-locked lasers a major limitation is the low damage threshold of the graphene layers, being on the order of 12 $mJ \cdot cm^{-2}$ for pulses of 50-fs duration [41] here, it is not expected to become an issue due to the high operating repetition rates.

Sources such as the femtosecond Ti:sapphire lasers reported here, with optimized operating characteristics can be appealing for frequency domain OCT, particularly the spectrometer based SDOCT variant, which is predominantly applied for dental and ophthalmic applications. The small footprint of the Ti:sapphire sources in combination with the development of semiconductor diode laser pumping schemes for Ti:sapphire lasers[42-44] and the progress in the design and technology of on-chip integration of OCT components, on various platforms

including silicon[45-47], lithium niobate-on- silicon[48], and silicon oxynitride[49] are relevant to further the development of miniaturized OCT instruments. Considering the inherent potential of the direct ultra-short pulse writing technique for development of arrays of closely spaced channel waveguides in a host crystal, one could envisage the use of ensembles of mode-locked waveguide lasers, similar to the ones reported here, for the realization of rapid in-vivo scanning in parallel OCT schemes[50]. In this context, the ultra-short pulse laser technique can also be exploited for the development of integrated interleaver devices in the bulk of a host material provided that propagation loss can be maintained at low levels.

The concept of coherent pulse interleaving and generation of phase-coherent pulsed output demonstrated here can be applied for low-phase noise microwave signal generation[51] and also be of great value for telecommunication applications, if realized in conjunction with mode-locked waveguide lasers operating in any of the telecom wavelength windows. As an example, miniature multi-gigahertz mode-locked sources coupled to suitably designed interleaver filters that incorporate thermal tuning modalities and can establish a differential delay to remain aligned to the ITU grid are useful for optical division multiplexing systems.[52,53] Improvements in the quality of the waveguides in terms of propagation loss and the ensuing increase in the average power generated can pave the way for further repetition rate scaling through a larger number of interleaver stages and broaden the range of applications that can be addressed. Finally, the stability of the phase-coherent output from the interleaver suggests the possibility of generation of dual optical frequency combs for spectroscopic applications[54,55] using configurations that involve the coupling of the laser output into two separate interleavers.

Supporting information

Additional supporting information on the (i) propagation loss in Ti:sapphire waveguides and emission beam quality factors of the respective lasers, (ii) fabrication and characterization of the

GSAs and (iii) dependence of the intracavity GDD on the gap size of the GTI may be found in the online version of this article at the publisher's website.

Figure S1: **Material and optical characteristics of the graphene layers. (a)** Raman spectrum of the GSA generated through laser excitation at 514.5 nm. **(b)** Linear transmission of the GSA as a function of wavelength, indicating a transmission value of T_{lin} = 96.1 at the mode-locked laser operating wavelength of 798.5 nm. **(c)** Time-resolved pump-probe measurements in the GSA indicating the existence of relaxation channels with corresponding constants of 207.4 fs and 1.45 ps.

Figure S2: **Intracavity GDD generated by the GTI. (a)** Calculated intracavity GDD for a wavelength of 798.5 nm as a function of size of the GTI air-filled gap with a refractive index of 1, indicating the intracavity GDD levels that can be established. **(b)** Zoom-in of (a) along with the corresponding GDD levels established with the GTI in the cavities of the mode-locked channel waveguide lasers developed in the femtosecond (red line) and picosecond (cyan line) regimes. The intersecting points correspond to gap sizes that can lead to stable mode-locking.

Acknowledgments: PL and GB acknowledge the support of the UK's Engineering and Physical Sciences Research Council (EPSRC) through the grants EP/M025330/1 and EP/L01243X/1, respectively. CCH and DBH acknowledge in part sponsoring by the EPSRC through the National Hub in High Value Photonic Manufacturing (EP/N00762X/1 grant).

Keywords: ultrafast lasers, soliton mode-locking, channeled waveguides, frequency combs, optical coherence tomography

Conflict of interest

The authors declare no conflict of interest.

FIGURE CAPTIONS

C. Grivas et. al. *"Generation of multi-gigahertz …… waveguides"*

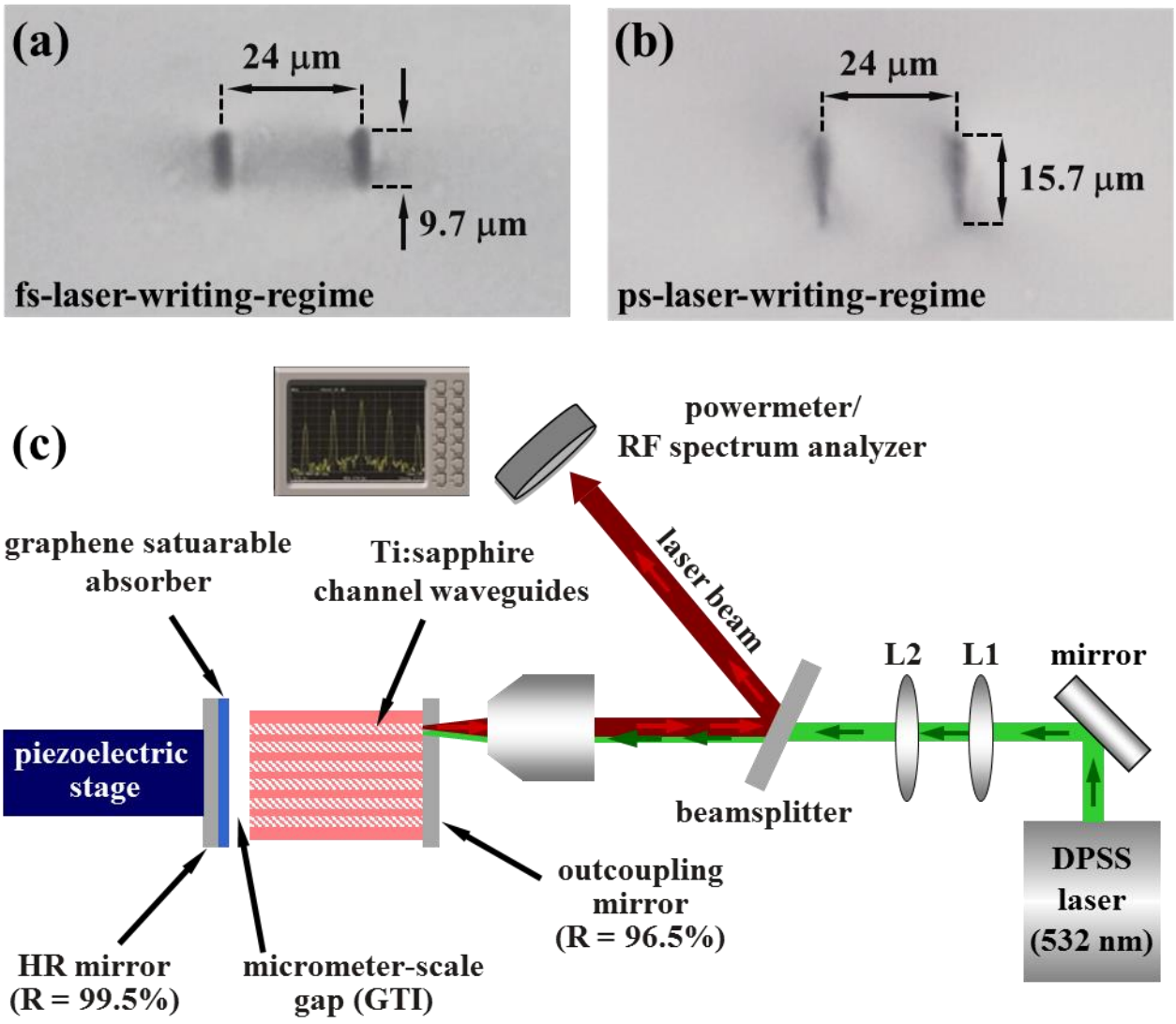

Figure 1. Ti:sapphire channel waveguides and experimental setup for their soliton mode-locking: Cross sectional microscope images of waveguides inscribed by **(a)** fs laser irradiation (180 fs, 1 kHz, 1030 nm) and **(b)** ps laser irradiation (8 ps, 200 kHz, 1064 nm). **(c)** In the experimental setup, the saturable absorber, a graphene layer deposited on an HR mirror attached to a piezoelectric stage, formed a GTI interferometer with the waveguide endface. Modulation of the micrometer size separation between the saturable absorber and the waveguide endface via the piezoelectric stage provided a means of dispersion engineering in the cavity, allowing for the formation of pulses with femtosecond duration.

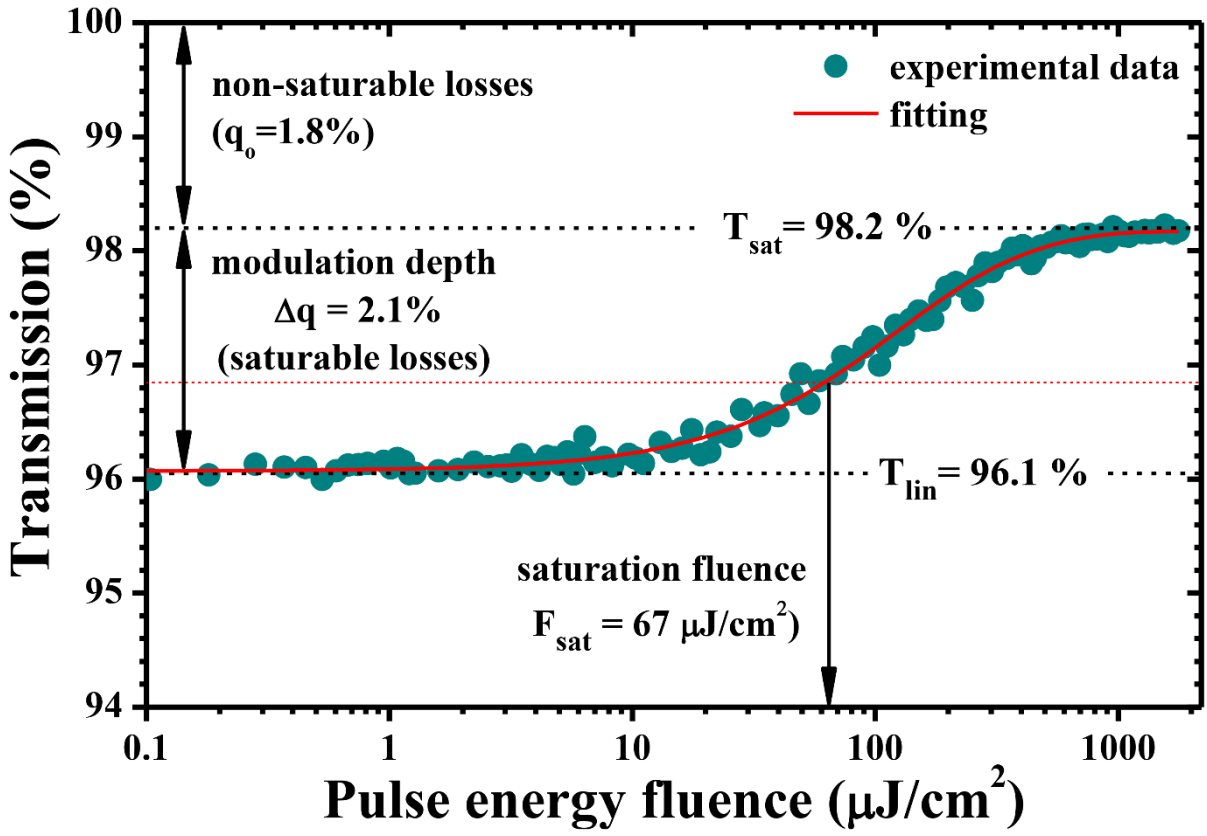

Figure 2. Parameters of the graphene saturable absorber. Transmission measurements of the graphene saturable absorber layer as a function of pulse energy fluence to determine operating parameters of the device such as its saturation fluence (67 $\mu J \cdot cm^{-2}$), modulation depth (2.1%) and non-saturable loss (1.8%).

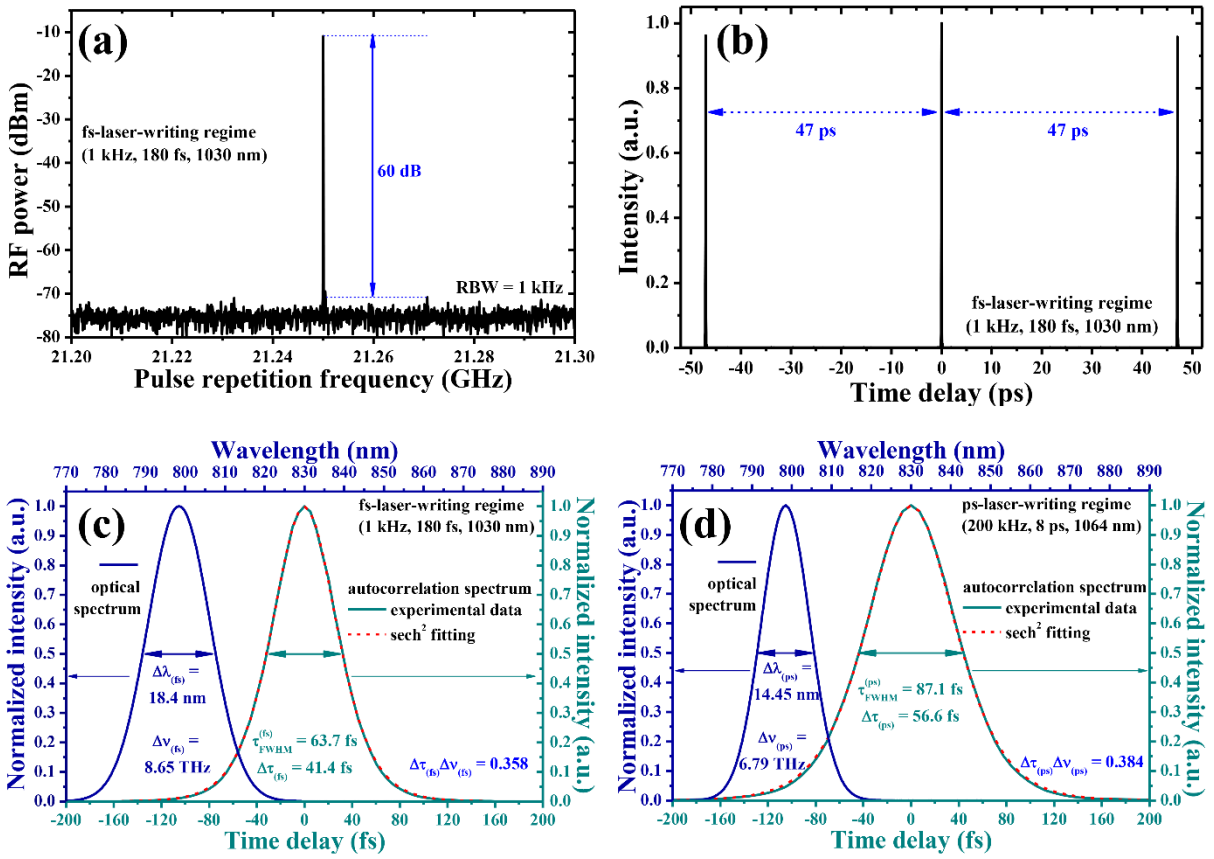

Figure 3. Characterization of the soliton mode-locked pulses: **(a)** RF spectrum at the fundamental repetition frequency indicating a signal-to-background suppression of 60 dB. **(b)** Autocorrelation trace of the 21.25 GHz pulse train, indicating a separation between successive pulses of 47.06 ps. **(c, d)** Autocorrelation traces and optical spectra of the pulsed output from the mode-locked Ti:sapphire channel waveguide lasers fabricated by femtosecond **(c)** and picosecond **(d)** laser writing. The red dashed lines represent $sech^2$ fittings to the autocorrelation traces recorded. The pulses generated were near-transform-limited as their pulsewidths ($\Delta\tau$) and optical bandwidths ($\Delta\nu$) yielded time-bandwidth products ($\Delta\tau\cdot\Delta\nu$) of 0.358 and 0.384 in the two writing regimes, respectively.

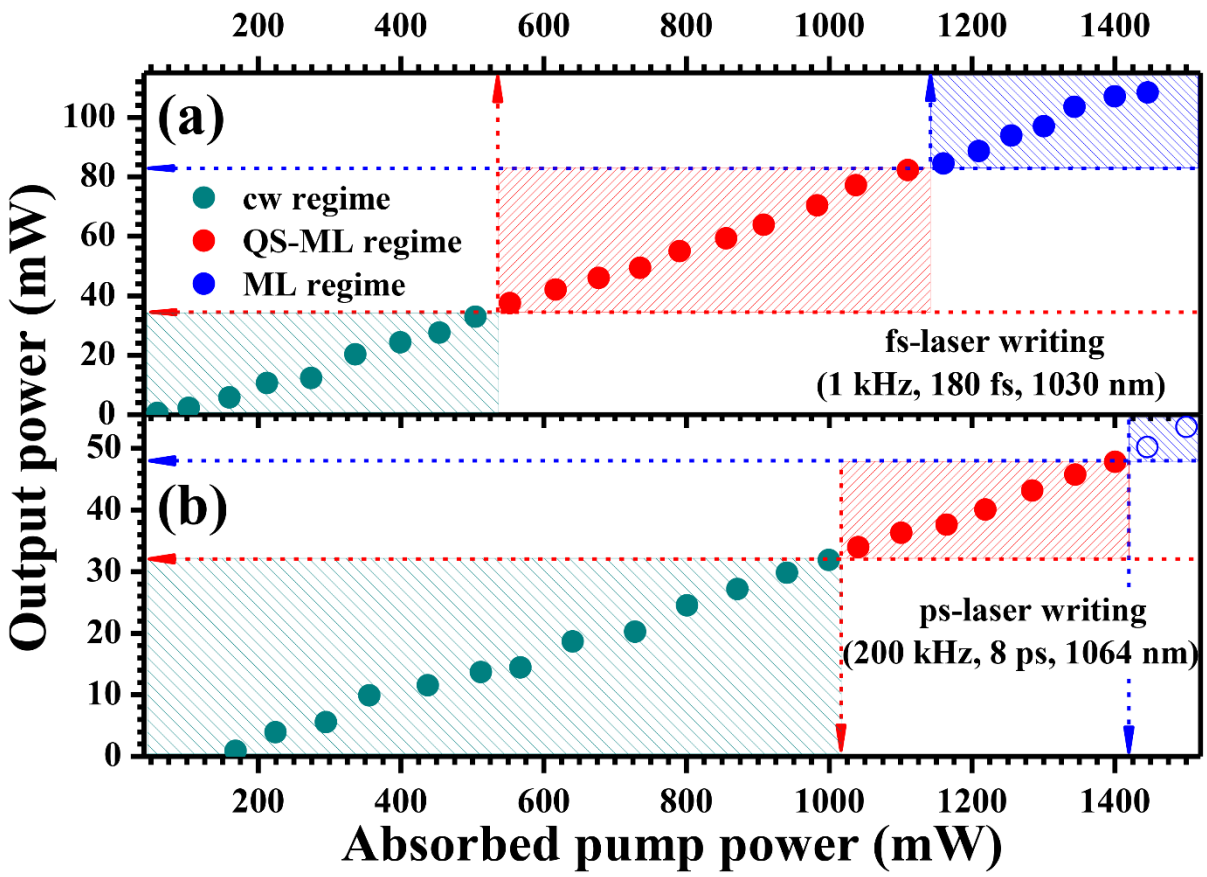

Figure 4. Laser input-output characteristics: Average output power as a function of absorbed pump power for waveguide lasers fabricated in the **(a)** femtosecond- and **(b)** picosecond-laser writing regime. The three laser operating regimes that were distinguished, namely c.w., Q-switched mode-locking (QSML), and mode-locking (ML) as well as the absorbed pump power ranges, in which they prevail are indicated by the colored shadowed areas, green (c.w.), red (QSML), and blue (ML).

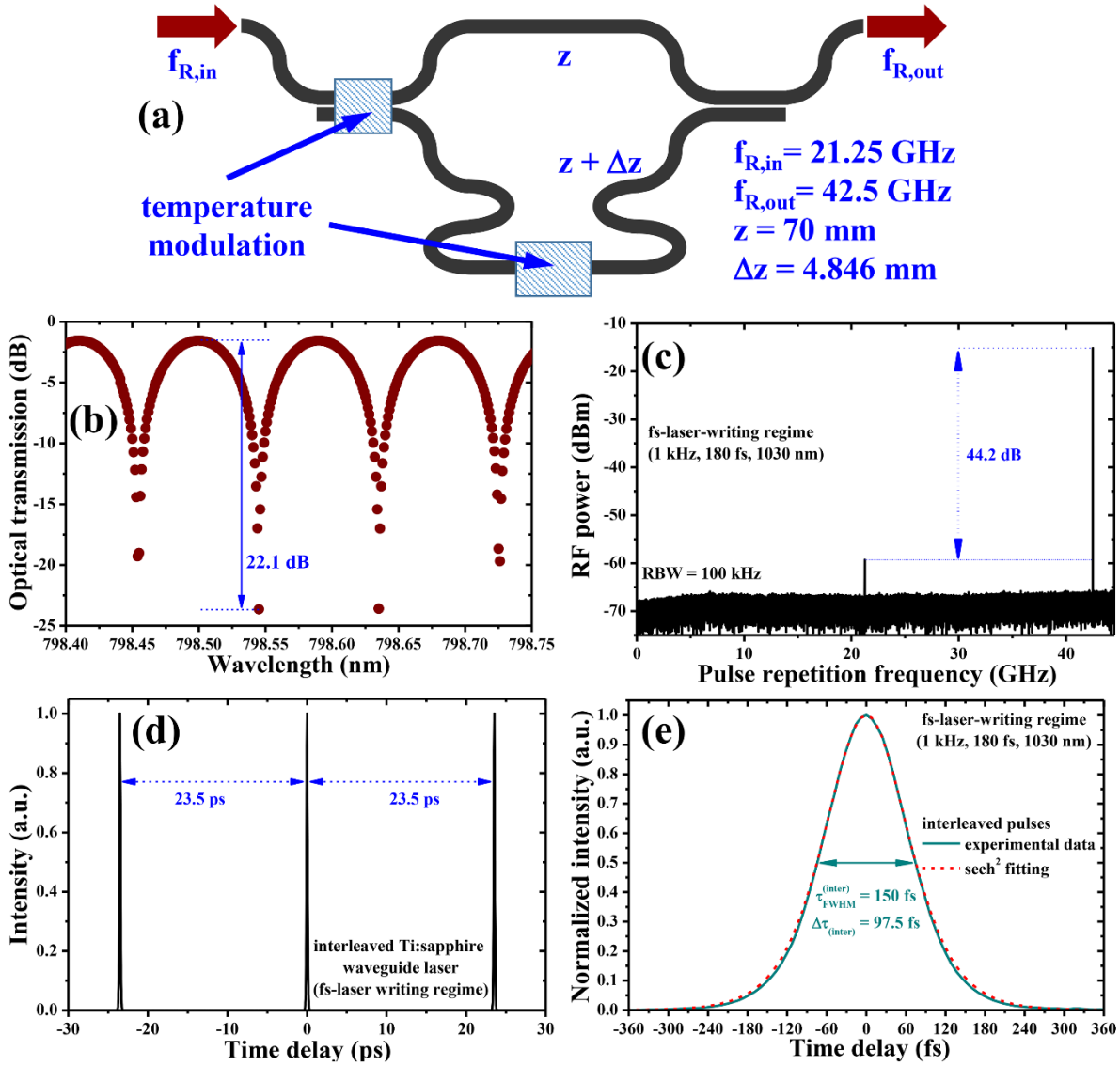

Figure 5. Rate multiplication via the fiber interleaver technology: (a) Schematic of the optical fiber interleaver layout, indicating the areas where thermal tuning was applied to optimize the coupling ratio of the directional coupler and delay line length of the MZI. **(b)** Measured optical transmission through the thermally-tuned interleaver filter, showing a suppression of 22.1 dB. **(c)** RF spectrum indicating a 44.2-dB suppression for the 42.5-GHz laser output by thermal tuning of the interleaver **(d)** Autocorrelation trace of the 42.5 GHz pulse train including cross-correlations. The distance between the peaks was ~ 23.5 ps, which corresponds to a repetition rate of 42.5 GHz. **(e)** autocorrelation trace of the interleaved pulses along with the $sech^2$ fitting (red dashed lines), indicating an FWHM duration of 150 fs, which corresponds to a pulsewidth, $\Delta\tau_{(inter)}$, of 97.5 fs.

References

[1] P. F. Moulton, "Spectroscopic and laser characteristics of Ti:Al_2O_3," J. Opt. Soc. Am. B **3**, 125–133 (1986).

[2] T. Südmeyer, S. V. Marchese, S. Hashimoto, C. R. E. Baer, G. Gingras, B. Witzel, U. Keller, "Femtosecond laser oscillators for high-field science," Nat. Photonics **2**, 599–604 (2008).

[3] U. Morgner, F. X. Kärtner, S. H. Cho, Y. Chen, H. A. Haus, J. G. Fujimoto, E. P. Ippen, V. Scheuer, G. Angelow, T. Tschudi, "Sub-two-cycle pulses from a Kerr-lens mode-locked Ti:sapphire laser," Opt. Lett. **24**, 411–413 (1999).

[4] R. Ell, U. Morgner, F. X. Kärtner, J. G. Fujimoto, E. P. Ippen, V. Scheuer, G. Angelow, T. Tschudi, M. J. Lederer, A. Boiko, B. Luther-Davies, "Generation of 5-fs pulses and octave-spanning spectra directly from a Ti:sapphire laser," Opt. Lett. **26**, 373 (2001).

[5] D. H. Sutter, G. Steinmeyer, L. Gallmann, N. Matuschek, F. Morier-Genoud, U. Keller, V. Scheuer, G. Angelow, T. Tschudi, "Semiconductor saturable-absorber mirror assisted Kerr-lens mode-locked Ti:sapphire laser producing pulses in the two-cycle regime," Opt. Lett. **24**, 631–633 (1999).

[6] A. A. Anderson, R. W. Eason, L. M. B. Hickey, M. Jelinek, C. Grivas, D. S. Gill, N. A. Vainos, "Ti:sapphire planar waveguide laser grown by pulsed laser deposition," Opt. Lett. **22**, 1556–1558 (1997).

[7] C. Grivas, D. P. Shepherd, T. C. May-Smith, R. W. Eason, M. Pollnau, A. Crunteanu, M. Jelinek, "Performance of Ar+-milled Ti:sapphire rib waveguides as single transverse-mode broadband fluorescence sources," IEEE J. Quantum Electron. **39**, 501–507 (2003).

[8] C. Grivas, D. P. Shepherd, T. C. May-Smith, R. W. Eason, M. Pollnau, "Single-transverse-mode Ti:sapphire rib waveguide laser," Opt. Express **13**, 210–215 (2005).

[9] C. Grivas, D. P. Shepherd, R. W. Eason, L. Laversenne, P. Moretti, C. N. Borca, and M. Pollnau, "Room-temperature continuous-wave operation of Ti:sapphire buried channel-waveguide lasers fabricated via proton implantation," Opt. Lett. **31**, 3450–3452 (2006).

[10] C. Grivas, C. Corbari, G. Brambilla, P. G. Lagoudakis, "Tunable, continuous-wave Ti:sapphire channel waveguide lasers written by femtosecond and picosecond laser pulses," Opt. Lett. **37**, 4630–4632 (2012).

[11] Y. Ren, Y. Jiao, J. R. Vázquez de Aldana, F. Chen, "Ti:Sapphire micro-structures by femtosecond laser inscription: Guiding and luminescence properties," Opt. Mater. **58**, 61–66 (2016).

[12] S. C. Wang, T. I. Yang, D. Y. Jheng, C. Y. Hsu, T. Te Yang, T. S. Ho, S. L. Huang, "Broadband and high-brightness light source: glass-clad Ti:sapphire crystal fiber," Opt. Lett. **40**, 5594–5597 (2015).

[13] S. C. Wang, C.-Y. Hsu, T.-T. Yang, D.-Y. Jheng, T.-I. Yang, T.-S. Ho, S.-L. Huang, "Laser-diode pumped glass-clad Ti:sapphire crystal fiber laser," Opt. Lett. **41**, 3217–3220 (2016).

[14] C. Grivas, "Optically pumped planar waveguide lasers: Part II: Gain media, laser systems, and applications," Prog. Quantum Electron. **45**, 3–160 (2016).

[15] J. Fujimoto, E. Swanson, "The Development, Commercialization, and Impact of Optical Coherence Tomography," Investig. Opthalmology Vis. Sci. **57**, OCT1 (2016).

[16] W. Drexler, M. Liu, A. Kumar, T. Kamali, A. Unterhuber, R. A. Leitgeb, "Optical coherence tomography today: speed, contrast, and multimodality," J. Biomed. Opt. **19**, 071412 (2014).

[17] A. F. Fercher, "Optical coherence tomography – development, principles, applications," Z. Med. Phys. **20**, 251–276 (2010).

[18] W. Drexler, U. Morgner, F. X. Kärtner, C. Pitris, S. A. Boppart, X. D. Li, E. P. Ippen, J. G. Fujimoto, "In vivo ultrahigh-resolution optical coherence tomography," Opt. Lett. **24**,

1221–1223 (1999).
[19] C. Hönninger, R. Paschotta, F. Morier-Genoud, M. Moser, U. Keller, "Q-switching stability limits of continuous-wave passive mode locking," J. Opt. Soc. Am. B **16**, 46–56 (1999).
[20] C. Grivas, "Optically pumped planar waveguide lasers, Part I: Fundamentals and fabrication techniques," Prog. Quantum Electron. **35**, 159–239 (2011).
[21] F. Chen, J. R. V. de Aldana, "Optical waveguides in crystalline dielectric materials produced by femtosecond-laser micromachining," Laser Photon. Rev. **8**, 251–275 (2014).
[22] T. Calmano, S. Muller, "Crystalline Waveguide Lasers in the Visible and Near-Infrared Spectral Range," IEEE J. Sel. Top. Quantum Electron. **21**, 401–413 (2015).
[23] Y. Ren, L. Zhang, H. Xing, C. Romero, J. R. Vázquez de Aldana, F. Chen, "Cladding waveguide splitters fabricated by femtosecond laser inscription in Ti:Sapphire crystal," Opt. Laser Technol. **103**, 82–88 (2018).
[24] A. Martinez and Z. Sun, "Nanotube and graphene saturable absorbers for fibre lasers," Nat. Photonics **7**, 842–845 (2013).
[25] I. H. Baek, H. W. Lee, S. Bae, B. H. Hong, Y. H. Ahn, D.-I. Yeom, and F. Rotermund, "Efficient Mode-Locking of Sub-70-fs Ti:Sapphire Laser by Graphene Saturable Absorber," Appl. Phys. Express **5**, 032701 (2012).
[26] A. Choudhary, A. A. Lagatsky, P. Kannan, W. Sibbett, C. T. A. Brown, D. P. Shepherd, "Diode-pumped femtosecond solid-state waveguide laser with a 4.9 GHz pulse repetition rate," Opt. Lett. **37**, 4416–4418 (2012).
[27] A. G. Okhrimchuk, P. A. Obraztsov, "11-GHz waveguide Nd:YAG laser CW mode-locked with single-layer graphene," Sci. Rep. **5**, 11172 (2015).
[28] A. A. Lagatsky, A. Choudhary, P. Kannan, D. P. Shepherd, W. Sibbett, C. T. A. Brown, "Fundamentally mode-locked, femtosecond waveguide oscillators with multi-gigahertz repetition frequencies up to 15 GHz," Opt. Express **21**, 19608–19614 (2013).
[29] R. Wessel, R. Ricken, K. Rochhausen, H. Suche, W. Sohler, "Supermode stabilized coupled-cavity 5- and 10-GHz mode-locked Ti:Er:LiNbO3 waveguide lasers," IEEE J. Quantum Electron. **36**, 394–399 (2000).
[30] P. G. Kazansky, Y. Shimotsuma, J.R. Qiu, K. Hirao "Self-Organized Nanogratings in Glass Irradiated by Ultrashort Light Pulses," Phys. Rev. Lett. **91,** 247405 (2003)
[31] J. D. Mills, P.G. Kazansky, E. Bricchi, J. J. Baumberg, "Embedded anisotropic microreflectors by femtosecond-laser nanomachining," Appl. Phys. Lett. **81,** 196 (2002).
[32] D. Wortmann, J. Gottmann, N. Brandt, H. Horn-Solle, "Micro- and nanostructures inside sapphire by fs-laser irradiation and selective etching," Opt. Express **16,** 1517–1522 (2008).
[33] J. Bai, G.H Cheng, X.W. Long, Y.S Wang, W. Zhao, G.F Chen, R. Stoian, R.Q Hui "Polarization behavior of femtosecond laser written optical waveguides in Ti:Sapphire," Opt. Express **20,** 15035-15044 (2012)
[34] W. Yang, P. G. Kazansky, Y. P. Svirko, "Non-reciprocal ultrafast laser writing," Nat. Photonics **2,** 99–104 (2008).
[35] J. Kuhl, J. Heppner, "Compression of femtosecond optical pulses with dielectric multilayer interferometers," IEEE J. Quantum Electron. **22**, 182–185 (1986).
[36] T. A. Birks, "Twist-induced tuning in tapered fiber couplers," Appl. Opt. **28**, 4226–4233 (1989).
[37] D. Pudo, H. Byun, J. Chen, J. Sickler, F. X. Kärtner, E. P. Ippen, "Scaling of passively mode-locked soliton erbium waveguide lasers based on slow saturable absorbers," Opt. Express **16**, 19221–19231 (2008).
[38] H. Byun, D. Pudo, S. Frolov, A. Hanjani, J. Shmulovich, P. Ippen, E, F. X. Kärtner, "Integrated Low-Jitter 400-MHz Femtosecond Waveguide Laser," IEEE Photonics

Technol. Lett. **21**, 763–765 (2009).
[39] E. Fedulova, K. Fritsch, J. Brons, O. Pronin, T. Amotchkina, M. Trubetskov, F. Krausz, V. Pervak, "Highly-dispersive mirrors reach new levels of dispersion," Opt. Express **23,** 13788–13793 (2015)
[40] P. Dombi, P. Rácz, M. Lenner, V. Pervak, F. Krausz "Dispersion management in femtosecond laser oscillators with highly dispersive mirrors," Opt. Express **17,** 20598–20604 (2009)
[41] M. Currie, J. D. Caldwell, F. J. Bezares, J. Robinson, T. Anderson, H. Chun, M. Tadjer "Quantifying pulsed laser induced damage to graphene" Appl. Phys. Lett **99,** 211909 (2011)
[42] P. W. Roth, A. J. Maclean, D. Burns, A. J. Kemp, "Directly diode-laser-pumped Ti:sapphire laser," Opt. Lett. **34**, 3334–3336 (2009).
[43] P. W. Roth, A. J. Maclean, D. Burns, A. J. Kemp, "Direct diode-laser pumping of a mode-locked Ti:sapphire laser," Opt. Lett. **36**, 304–306 (2011).
[44] K. Gürel, V. J. Wittwer, M. Hoffmann, C. J. Saraceno, S. Hakobyan, B. Resan, A. Rohrbacher, K. Weingarten, S. Schilt, T. Südmeyer, "Green-diode-pumped femtosecond Ti:Sapphire laser with up to 450 mW average power," Opt. Express **23**, 30043–30048 (2015).
[45] B. I. Akca, B. Považay, A. Alex, K. Wörhoff, R. M. de Ridder, W. Drexler, M. Pollnau, "Miniature spectrometer and beam splitter for an optical coherence tomography on a silicon chip," Opt. Express **21**, 16648–16656 (2013).
[46] G. Yurtsever, B. Považay, A. Alex, B. Zabihian, W. Drexler, R. Baets, "Photonic integrated Mach-Zehnder interferometer with an on-chip reference arm for optical coherence tomography," Biomed. Opt. Express **5**, 1050–1061 (2014).
[47] S. Schneider, M. Lauermann, P.-I. Dietrich, C. Weimann, W. Freude, C. Koos, "Optical coherence tomography system mass-producible on a silicon photonic chip," Opt. Express **24**, 1573–1586 (2016).
[48] B. I. Akca, "Design of a high-speed multiple-reference optical coherence tomography system," Opt. Express **24**, 26709–26714 (2016).
[49] V. D. Nguyen, B. I. Akca, K. Wörhoff, R. M. de Ridder, M. Pollnau, T. G. van Leeuwen, J. Kalkman, "Spectral domain optical coherence tomography imaging with an integrated optics spectrometer," Opt. Lett. **36**, 1293–1295 (2011).
[50] S. Bourquin, L. Laversenne, S. Rivier, T. Lasser, R.-P. Salathé, M. Pollnau, C. Grivas, D. P. Shepherd, R. W. Eason, "Parallel broadband fluorescent light source for optical coherence tomography," Proc. SPIE - Prog. Biomed. Opt. Imaging, **5690**, 209–213 (2005).
[51] S. A. Diddams, M. Kirchner, T. Fortier, D. Braje, A. M. Weiner, L. Hollberg, "Improved signal-to-noise ratio of 10 GHz microwave signals generated with a mode-filtered femtosecond laser frequency comb," Opt. Express **17**, 3331–3340 (2009).
[52] M. Y. Sander, S. Frolov, J. Shmulovich, E. P. Ippen, F. X. Kärtner, "10 GHz femtosecond pulse interleaver in planar waveguide technology," Opt. Express **20**, 4102–4113 (2012).
[53] S. Cao, J. Chen, J. N. Damask, C. R. Doerr, L. Guiziou, G. Harvey, Y. Hibino, H. Li, S. Suzuki, K. Y. Wu, P. Xie, "Interleaver Technology: Comparisons and Applications Requirements," J. Light. Technol. **22**, 281–289 (2004).
[54] I. Coddington, N. Newbury, W. Swann, "Dual-comb spectroscopy," Optica **3**, 414–426 (2016).
[55] S. M. Link, D. J. H. C. Maas, D. Waldburger, U. Keller, "Dual-comb spectroscopy of water vapor with a free-running semiconductor disk laser," Science **356**, 1164–1168 (2017).